ORIGINAL PAPER

Crystal structure, supramolecular assembly exploration by Hirshfeld surface analysis and DFT inspection of the synthesized functionalized crystalline anilide

Muhammad Ashfaq[1] · Muhammad Nawaz Tahir[1] · Georgii Bogdanov[2] · Akbar Ali[3] · Muhammad Ahmed[1] · Gulzar Ahmed[4] · Anees Abbas[5]

Abstract

The current research work is about the synthesis of functionalized crystalline anilide, i.e., (Z)-4-((2-nitrophenyl)amino)-4-oxobut-2-enoic acid (**NAOB**) and its experimental and theoretical investigation. The single-crystal X-rays diffraction technique is employed for the crystal structure determination. The crystal structure of **NAOB** is compared with two closely related crystal structures of the literature that contain nitro group at the para position of the phenyl ring. The supramolecular assembly was thoroughly explored by Hirshfeld surface analysis. The most probable contact for the crystal packing interactions was determined by enrichment ratio analysis. The crystal packing environment was explored by the interaction energy between the molecular pairs. Energy frameworks were computed to understand the topology of the single crystal of the compound **NAOB**. Void analysis was performed to check the strength of the crystal packing. In order to visualize the relative polarity and active sites of crystal structure, molecular electrostatic potential (MEP) study was performed. The DFT-based calculated results were found in agreement with the experimental results.

Graphical abstract
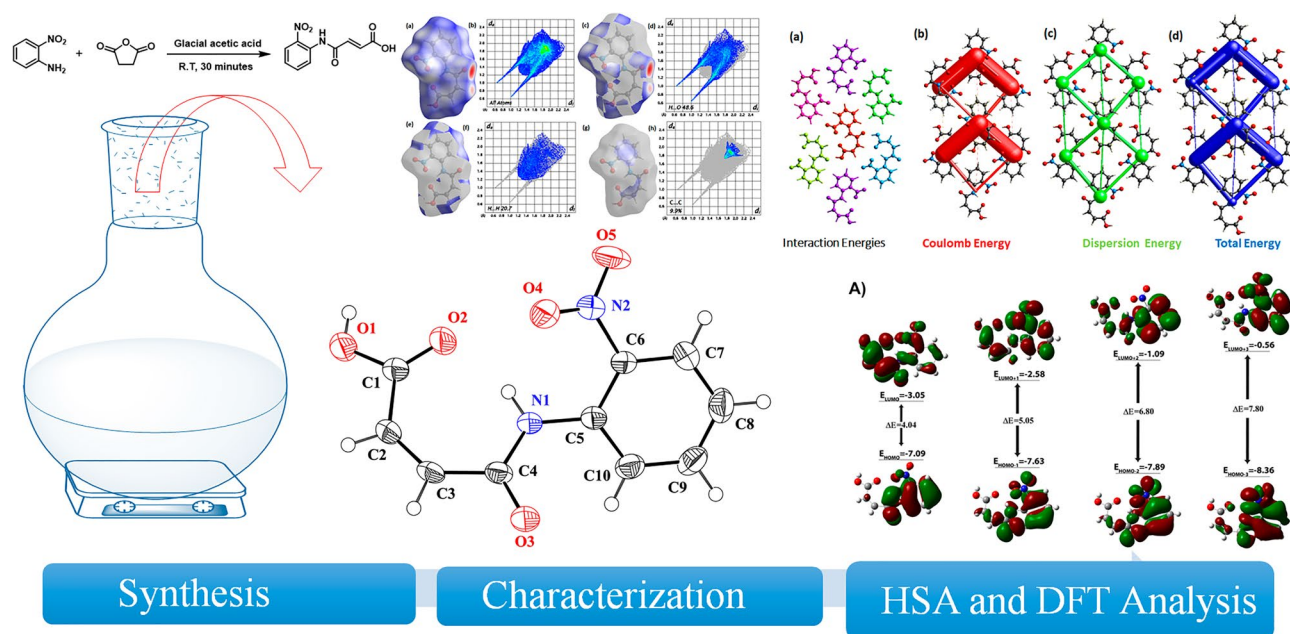
Extended author information available on the last page of the article

Introduction

Anilides accompanied by the carboxylic acid and their derivatives denote significant class of important organic compounds. Currently, these versatile compounds have attracted substantial attention due to their interesting pharmacological medications including treatment of tuberculosis (Mycobacterium tuberculosis and tubercle bacillus that are accountable for the leading cause of death worldwide), cancer and ulcer [1–3]. It is important to mention that, an extreme decline has been observed in the number of TB cases, courtesy to the discovery of effective anti-mycobacterial agents including isoniazid, ethambutol, rifampicin, pyrazinamide, and streptomycin. Functionalized anilide such as **NAOB** having the nitro group and carboxylic acid functionality could be interesting chemical architecture as the presence of many hetero atoms might be responsible for non-covalent interactions and could also be used as potential ligand in coordination chemistry for the production of metal–organic framework (MOFs) [4–6]. For instance, the similar structural pattern can be found in many important biologically active compounds having potential activities like anticancer and antidepressant [7, 8], antimicrobial and analgesic. Similarly, carboxamides and analogs having structural similarity to the **NAOB**, could be used as activators of caspases and inducers of apoptosis [9]. Similar structural sequence could also be observed in the anti-inflammatory and antioxidant agents. Some of the chemical structures with potential anti-HIV-I activity has also a similar structural format (Fig. 1) [10].

The Hirshfeld surface analysis is an important tool that is used for the crystalline compounds to find the van der Waals interactions and hydrogen bonding [11–15]. These non-covalent interactions are considered to play the major role in the crystal packing [16–19]. Herein, we are presenting our findings regarding crystal structure, the supramolecular assembly exploration by Hirshfeld surface analysis and DFT inspection of the functionalized crystalline anilide (**NAOB**).

Experimental

Chemicals and instrumentation

The acetic acid and other chemical used for the synthesis and purification used were of highest grade and used as received without any further purification.

Synthetic procedure of NAOB

The compound **NAOB** (2*E*)-4-[((2-nitrophenyl)amino)]-4-oxobutanoic acid) was prepared using the general procedure of the literature [20]. Accordingly, equivalent molar quantities of 2-nitroaniline, i.e., $C_6H_6N_2O_2$ (1 mmol, 138 mg) and succinic anhydride, i.e., $(CH_2CO)_2O$ (1 mmol, 100 mg) in 10 mL of glacial acetic acid was stirred at room temperature for 30 min. The solid form was separated out from the reaction mixture via filtration, washed with hexane and dried. The crude product was recrystallized using methanol (Scheme 1).
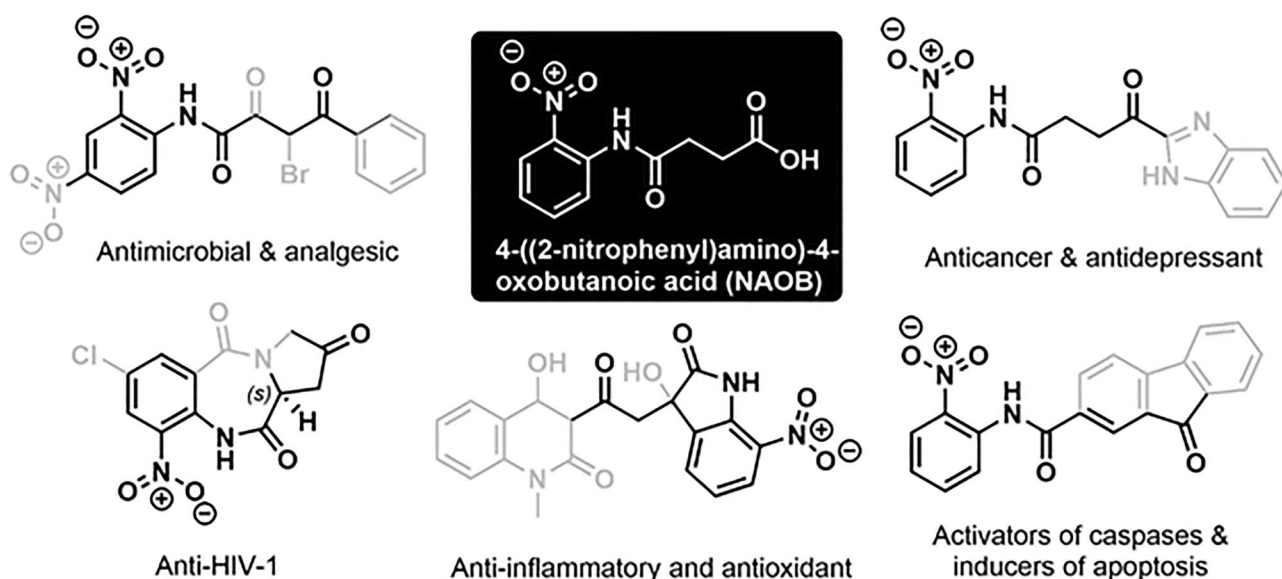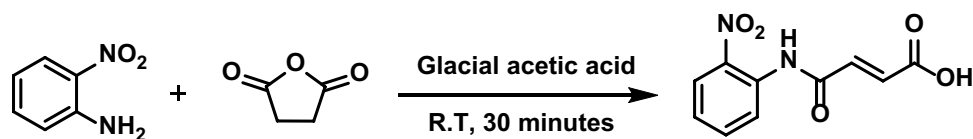

Fig. 1 **NAOB** resembled structures with their biological potential

Scheme 1 Synthesis of **NAOB** using 2-nitroaniline and succinic anhydride in acidic medium

Single Crystal XRD analysis details of NAOB

The single crystal XRD data of **NAOB** is collected on Bruker Kappa Apex-II diffractometer with APEX-II software for data collection. The absorption correction is performed on SADABS software. The SHELXT-2014 [21] and SHELXL 2019/2 [22] software are employed for structure solution and refinement, respectively. Anisotropic displacement parameters are assigned to all non-hydrogen atoms whereas isotropic displacement parameters are assigned to H-atoms. H-atoms are placed at the calculated positions by using riding model. ORTEP-3 [23] PLATON [24] and Mercury 4.0 [25] are used for the graphical representation of SC-XRD results.

Computational methodology

Density function theory (DFT) method was used to obtain the HOMO–LUMO energy values, using B3LYP method with the $6–311 + + G(d,p)$ basis set in Gaussian 16 and GaussView 6 software programs [26, 27]. First, after importing the experimental geometry, Gaussian optimization algorithm was used to obtain optimized geometry [28]. Next, Gaussian energy calculation algorithm was implemented to compute energy values for the frontier molecular orbitals, energy values of the whole structures, values of the dipole moment and visualization of the frontier molecular orbitals. Studies of the conceptual density functional theory (CDFT) were performed by using Multiwfn version 3.7 [29].

Result and discussion

The Cambridge structure database conformed that the crystal structure of **NAOB** is novel. The details related to single crystal X-Ray diffraction (SC-XRD) are listed in Table 1 whereas the important bond lengths and bond angles are listed in Table 2.

SC-XRD description of the crystal structure of NAOB.

In **NAOB** (Fig. 2, Table 1) the (Z)-4-amino-4-oxobut-2-enoic acid group A (C1-C4/N1/O1-O3) and phenyl ring B (C5-C10) are planar with root mean square (r.m.s.) deviation of 0.0639 and 0.0056 Å, respectively, with dihedral angle A/B of 38.8 (6)$^\circ$. The nitro group C (N2/O4/O5) is oriented at the dihedral angle of 42.8 (2)º relative to its parent group

Table 1 Experimental details related to SC-XRD for **NAOB**

Crystal data	**NAOB**
CCDC	2,190,922
Chemical formula	$C_{10}H_8N_2O_5$
M_r	236.18
Crystal system, space group	Monoclinic, $P2_1/n$
Temperature (K)	296 (2)
a, b, c (Å)	3.7505 (7), 22.663 (5), 11.828 (3)
α, β, γ°	90, 96.193 (6), 90
V (Å^3)	999.4 (4)
Z	4
Density (calculated)g/cm^{-3}	1.570
F(000)	488
Radiation type	Mo $K\alpha$
Wavelength (λ)	0.71073
μ (mm^{-1})	0.129
Crystal size (mm)	0.42×0.26×0.20
Data Collection	
Diffractometer	Bruker APEXII CCD diffractometer
Absorption correction	Multi-scan (SADABS; Bruker, 2007)
No. of measured, independent and observed [$I > 2\sigma(I)$] reflections	6807, 2136, 1285
R_{int}	0.055
Theta range for data collection (°)	1.951 to 26.883
Index ranges	$-4 \leq h \leq 3$, $-28 \leq k \leq 28$, $-14 \leq l \leq 14$
$(\sin θ/λ)_{max}$ (Å^{-1})	0.636
Data Refinement	
$R[F^2 > 2\sigma(F^2)]$, $wR(F^2)$, S	0.063, 0.169, 1.02
No. of reflections	2136
No. of parameters	155
H-atom treatment	H-atom parameters constrained
$\Delta\rho_{max}$, $\Delta\rho_{min}$ (e Å^{-3})	0.30, −0.25

Table 2 Selected bond lengths (Å) and bond angles (°) of **NAOB**

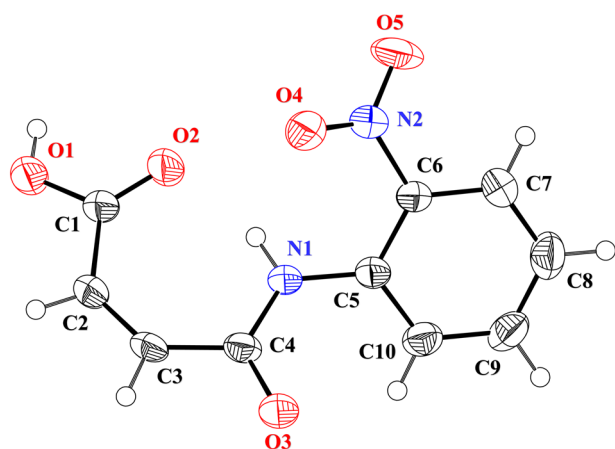| Selected bond lengths		Selected bond angles	
O1-C1	1.304 (3)	O1-C1-O2	122.0 (3)
O2-C1	1.204 (3)	O3-C4-N1	122.1 (3)
O3-C4	1.233 (3)	C4-N1-C5	125.6 (2)
N1-C4	1.342 (3)	O4-N2-O5	122.8 (3)
N1-C5	1.403 (3)	O4-N2-C6	119.1 (2)
O4-N2	1.218 (3)	O5-N2-C6	118.0 (3)
O5-N2	1.215 (3)		

Fig. 2 ORTEP diagram of **NAOB** that is drawn at probability level of 50%. H-atoms are shown by small circles of arbitrary radii

A. The deviation of O1-atom from plane of group A is larger than other atoms in the plane and deviation for O1-atom is 0.1157 (2) Å. The selected bond lengths and bond angles are listed in Table 2. The O1-C1and O2-C1 bond lengths are 1.304 (3) and 1.204 (3) Å, respectively, which showed there is single bond between O1 and C1 atoms and double bond between O2 and C1 atoms. The one of the O-atom of carboxylate group and one of O-atom of nitro group act as H-bond acceptor for NH group to form S (7) and S (6) H-bonded loops [30]. These intramolecular H-bonding are the main aspect of the molecular configuration for **NAOB**. The molecules are interlinked in the form of dimers through the combination of O–H···O and C–H···O bonding to form $R_2^2(8)$ loop [31] (Fig. 3, Table 3). C7 and C5 infinite chains are formed by O–H···O and C-H···O bonding, respectively. The one-dimensional chain network of molecules is formed with base vector [10 $\bar{1}$]. The crystal packing is further stabilized by the presence of off-set π···π stacking interaction [32] between phenyl rings of symmetry related molecules. The inter-centroid separation between interacting rings is

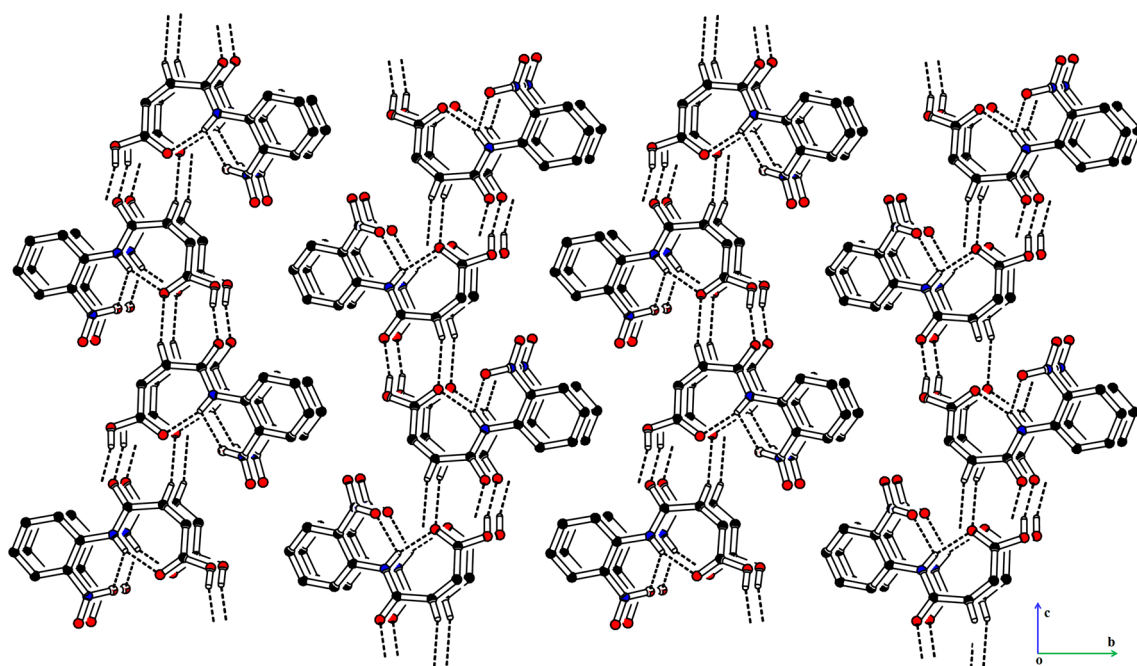**Fig. 3** Packing diagram of **NAOB**. Selected H-atoms are shown for clarity

Table 3 Hydrogen-bond geometry (Å, °) of **NAOB**

D—H···A	D—H	H···A	D···A	<(D—H···A)°
N1—H1A···O2	0.86	1.85	2.686 (3)	162
N1—H1A···O4	0.86	2.43	2.733 (3)	101
C3—H3···O2[i]	0.93	2.48	3.372 (3)	160
O1—H1···O3[ii]	0.82	1.82	2.624 (3)	166

3.751 (2) Å and ring off-set is 1.315 Å. Infinite chain of molecules is formed due to off-set π⋯π stacking interaction that runs along *a*-axis (Fig. 4).

It is possible to recognize the atom or a group of atoms of a molecule to be involved in intermolecular interactions. For the said purpose, we calculate the full interaction map. The main focus behind the full interaction map calculations is to visualize H-bond donors, H-bond acceptors, and the interactions that involve aromatic ring. The result of the full interaction map is shown in Fig. 5. The dark red region around the hydroxyl group indicates that it acts as a strong H-bond donor whereas the red region around NH group is light red indicates that it is a weak H-bond donor. It is evident from Table 3 that NH group is not engaged in any convection H-bonding, but it is involved in N–H ⋯ π interaction which is comparatively weaker than the convectional H-bonding. H-bond acceptors are indicted by blue regions around them. A pair light red region around aromatic ring indicated the involvement of the ring in π ⋯ π stacking interactions. The simulated powder X-ray diffraction (PXRD) pattern of **NAOB** is formed which inferred that there are three most intense peaks at positions 10.8°, 25.1° and 26.1° and labeled with corresponding hkl values (02 $\bar{1}$), (12 $\bar{1}$) and (11 $\bar{2}$), respectively (Fig. S1). These sharp peaks of **NAOB** indicate the high crystallinity of as prepared single crystal compound with no other impurities. The cambridge structure database [33] search inferred that the crystal structures with reference code JAYGEW [34] and MNPMAL01 [35] that have close similarity with the crystal structure of **NAOB**. The crystal structure of JAYGEW and MNPMAL01 have nitro group at the para position of the phenyl ring and both have one molecule in the asymmetric unit, crystallized in same crystal system and space group. The crystal structure with reference code JAYGEW and MNPMAL01 looks similar at
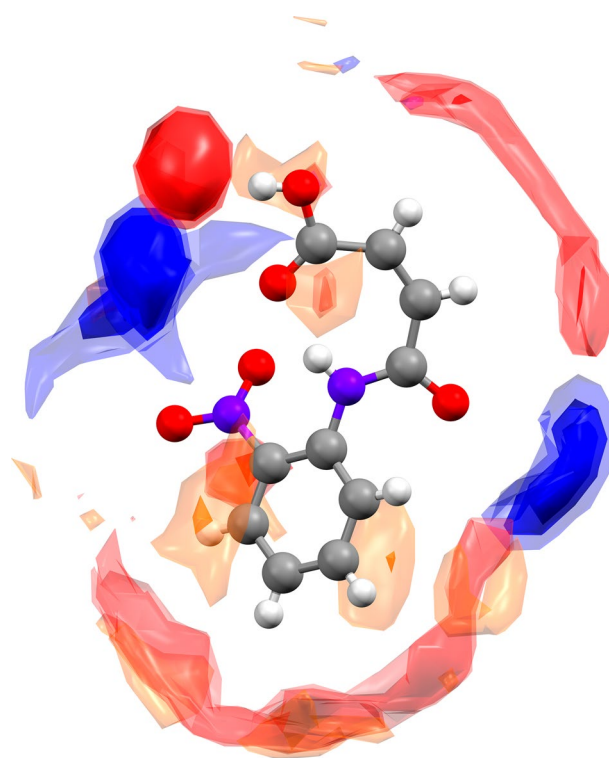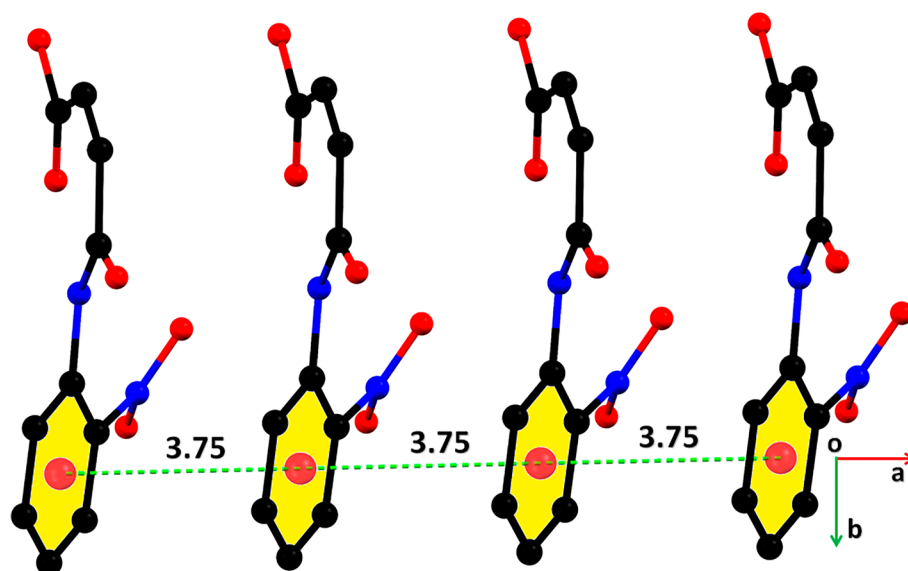

Fig. 5 Full interaction map of **NAOB**

first look. Both were crystallized in the same crystal system and space group but these structures are polymorphous. The crystal packing of JAYGEW and MNPMAL01 was different from one another. The molecules of JAYGEW were connected by N–H ⋯ O and C-H ⋯ O bonding in the form of chains of rings whereas the molecules of MNPMAL01 were interlinked by same H-bonding in the form sheets parallel to ($\bar{1}$ 01) plane.

Fig. 4 Graphical representation of off-set π ⋯ π stacking interaction in **NAOB**. H-atoms are not shown for clarity. Distances are measured in Å

Symmetry codes: (i) $x + 1/2, -y + 1/2, z - 1/2$; (ii) $x - 1/2, -y + 1/2, z + 1/2$.

Hirshfeld Surface Analysis

The intermolecular interactions in a single crystal of molecule were studied by Hirshfeld surface analysis on Crystal explorer 21.5 [36]. The concept of Hirshfeld surface (HS) arose when the researchers were trying to dissociate the crystal electron density into molecular fragments. Figure 6a is the Hirshfeld surface plotted over d_{norm} on which the red spots are the representatives of short contacts. White spots stand for the contacts for which the distance between the interacting atoms is equal to the sum of the Van der Waal radii of atoms whereas blue spots stand for the longer contacts [37–39]. Figure 6b, c shows the HS of **NAOB** along with d_e and d_i. Where d_e and d_i shows the distance from the Hirshfeld surface (HS) to the nearest nucleus external and internal to the surface, respectively. In order to visualize the $\pi \cdots \pi$ stacking interactions in **NAOB**, HS is plotted over curvedness (Fig. 6d) shape index (Fig. 6e). The large flat green region around the aromatic ring on the HS plotted over curvedness indicates the involvement of the aromatic ring in $\pi \cdots \pi$ stacking interactions. The presence of consecutive red and blue triangular regions around the aromatic ring also indicates the involvement of the aromatic ring in $\pi \cdots \pi$ stacking interactions. Close contacts with neighbor atoms from inside to outside $O \cdots H$ and $H \cdots O$ are represented in Fig. 6f on which the red color circles revealed the hydrogen bonding contacts and blue regions show the longer contacts on the HS surface.

The 2D fingerprint plots (Fig. 7) were provided for additional information about the intermolecular interactions. It provides direct insight of the supramolecular assembly in the single crystals [40–42]. The analysis inferred that $H \cdots O$, $H \cdots H$ and $C \cdots C$ as major contributors for the crystal packing. The highest contribution was found 48.5% for $H \cdots O$ to the crystal packing and 20.7% for $H \cdots H$ followed by $C \cdots C$ 9.9%. Other contacts or interactions were negligible and are given in supporting information.

Molecular Electrostatic Potential (MEP)

MEP is the method to visualize relative polarity and active sites of crystal structure, this is effective way to investigate reactivity and the relative polarity of molecule [43–45]. Figure 8 shows the 3D MEP maps of **NAOB**, the negative potential represented by red regions are mainly localized over the terminal oxygen atoms of **NAOB** anion. So red regions are most suitable positions for electrophilic attack in the **NAOB**. The blue region represents the positive potential region of **NAOB** that indicates possible sites for nucleophilic attack.

Fig. 6 Hirshfeld surface map of **NAOB**: **a** dnorm, **b** de, **c** di, **d** shape index, **e** curvedness and **f** interactions with neighbor molecules $H \cdots O$ and $O \cdots H$ positions
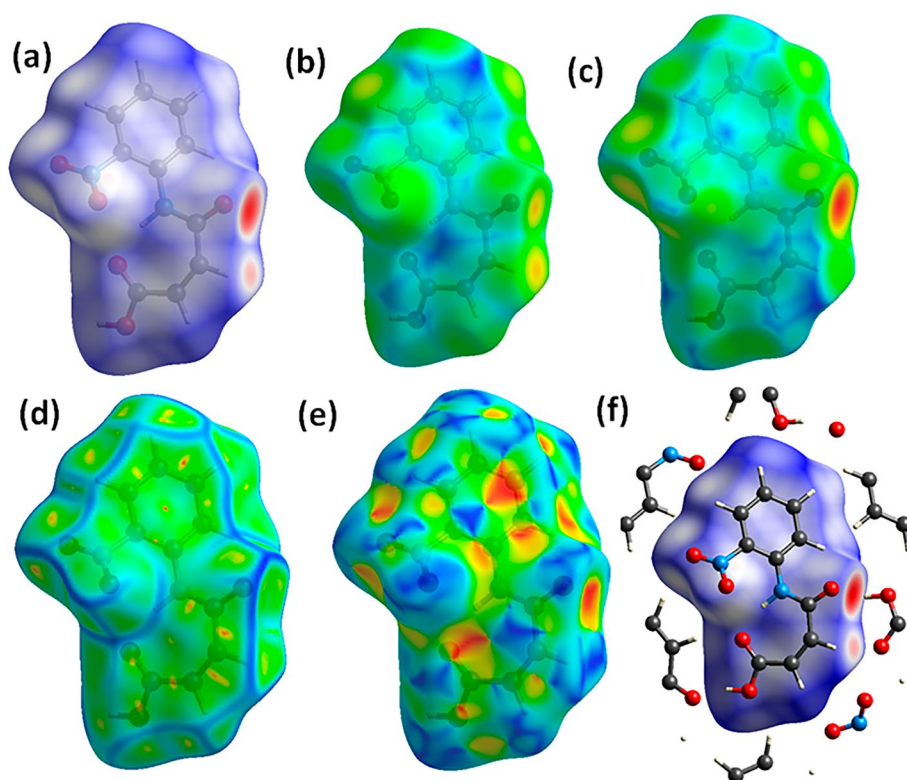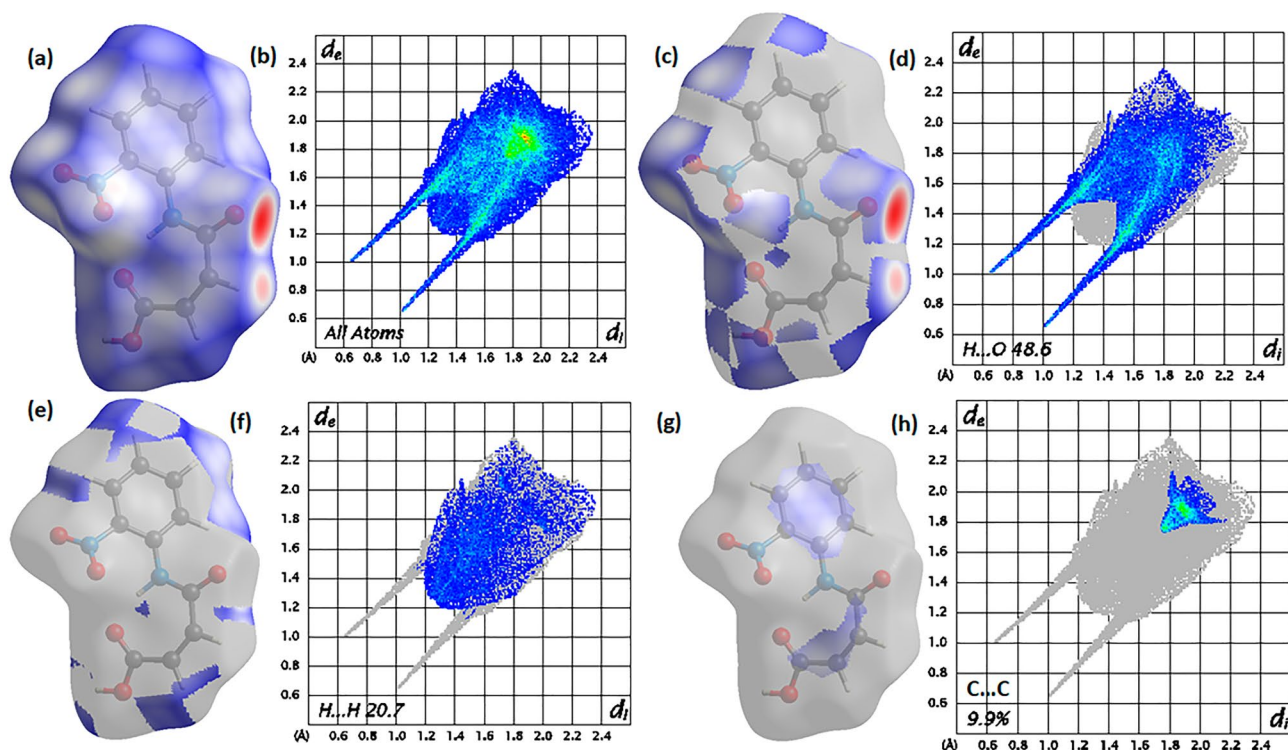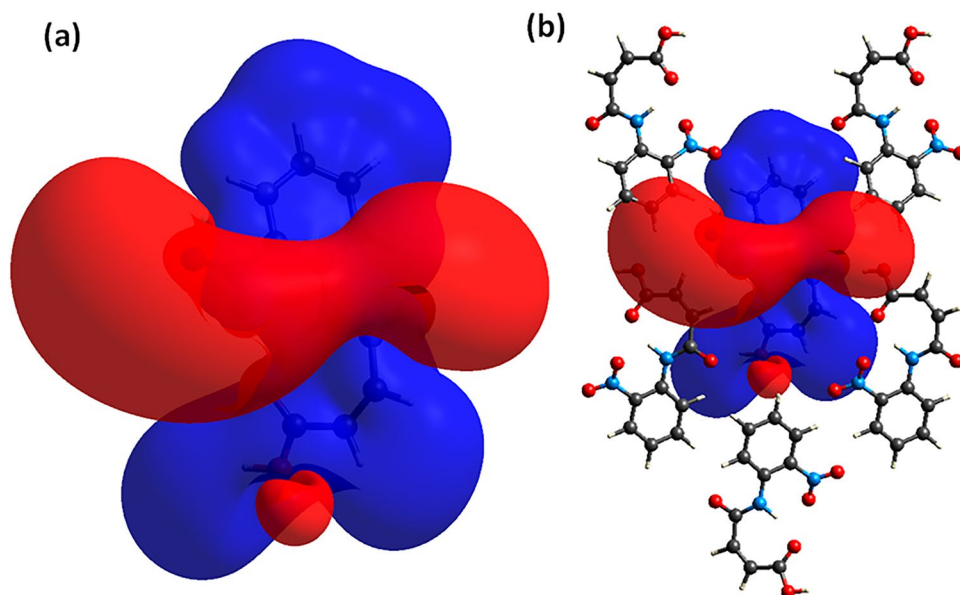
Fig. 7 Fingerprint plots of **NAOB**, **b** all atoms, **d** H ⋯ O (48.5%), **f** H ⋯ H (20.7%), **h** C ⋯ C (9.9%). Exact Position of interaction represented by **a, c, e, g**

Fig. 8 Molecular electrostatic potential (MEP) of **NAOB, a** The MEP on the HS with the property cloned to its nearest neighbors to identify the potential acceptor and donor sites, **b** The color range was chosen to be the −0.008 to +0.008 a.u

Void Analysis

Promolecular surfaces were used to visualize the size, shape and the space belong to molecule in crystal. Similarly, these surfaces can also be used to identify the region or space not related with a molecule or with molecules in a crystal. So,

crystal voids can be visualized by simply building an isosurface of the procrystal electron density. Figure 9 demonstrates the correlation between isosurface of the procrystal electron density and 0.002 au promolecule isosurfaces for **NAOB**. All the atoms are assumed to be spherically symmetric and electron density of all the atoms are added up in order to find

Fig. 9 Unit cell packing diagram for **NAOB a** with 0.002 au void surface **b** with combination with individual promolecule surfaces at 0.002 au
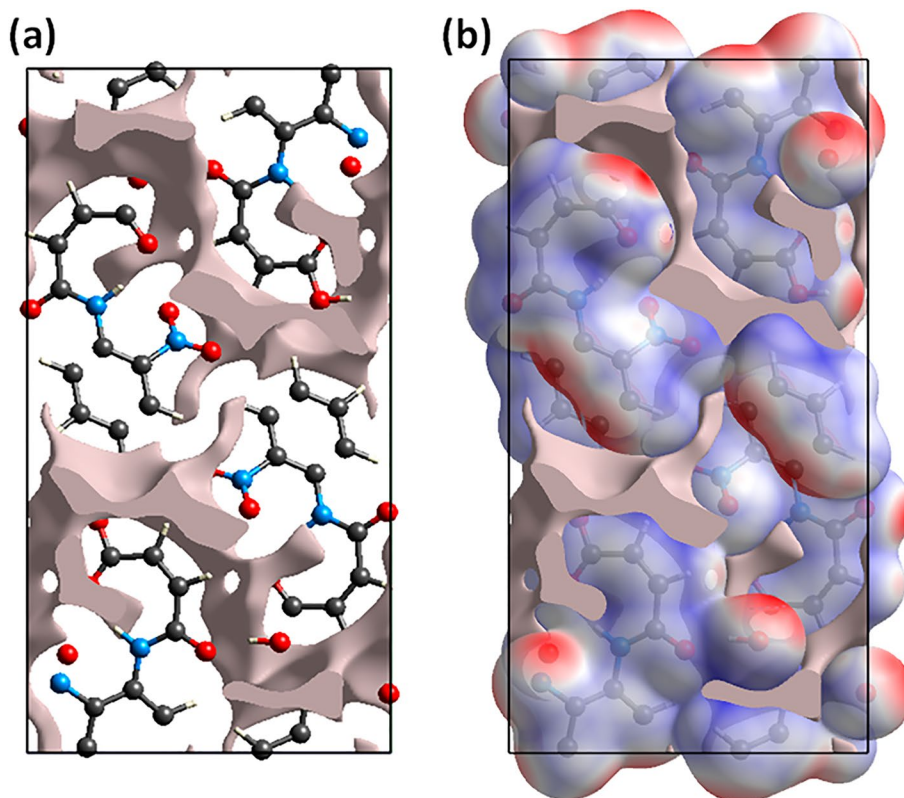
voids [46–48]. We found the void surface with volume of 79.77 Å^3 per unit cell and total cell volume was found 999.4 Å^3 which inferred that the molecules are strongly packed as the void occupy just 7.98% of the space of the unit cell. The promolecule isosurface for individual volume of **NAOB** was calculated 221.45 Å^3 (Fig. 9a). Figure 9b shows the electron densities overlap in the procrystal, the sum of their individual volumes for two molecules per unit cell was found 442.90 Å^3.

Interaction energy and energy frameworks

Interaction energies of **NAOB** were calculated with model B3LYP/6-31G(d,p)by using Crystal explorer version 21.5. The interaction energy is the sum of four kinds of energies named as electrostatic, dispersion, polarization and repulsion [49–51]. The interaction energy is calculated for the cluster of molecules that lie within 3.8 Å^3 volume of the reference molecule (Fig. 10a). The interaction energy calculations inferred that the interaction energy is greatest for the pair of molecules that are connected by symmetry (x + 1/2, -y + 1/2, z + 1/2) (Fig. 10e). Energy frameworks represents the strength of a particular kind of energy. The thickness of the cylinders is directly proportional to the strength of the particular kind of energy. The energy framework calculations inferred that the dispersion energy has greater

contribution as compared to the coulomb energy in defining the total interaction energy (Fig. 10b, c, d).

Computational results

DFT inspection

The application of density functional theory (DFT) delivers an extensive foundation that can be used to characterize various properties of the compound, including physical and chemical properties that can be used to predict how the single crystal structure will behave [52]. We can achieve that by determining the energies associated with molecular orbitals and the energy gaps between them. Energy gap, i.e., a minimum required energy for an electron to reach an excited state, ΔE (E_{LUMO}–E_{HOMO}), represents the reactive ability of molecules to interact with other molecules, (electrophiles or nucleophiles). A hard, less polarizable, and less reactive molecule has larger energy gap, when a soft, highly polarizable and higher chemically reactive molecule has smaller energy gap.

As a first step of the DFT analysis, geometry optimization to minimum energy state was performed for the title compound by applying B3LYP/6–311 + + G(d,p) method (Fig. 11). DFT calculations were performed on both experimentally obtained from X-Ray geometry and optimized
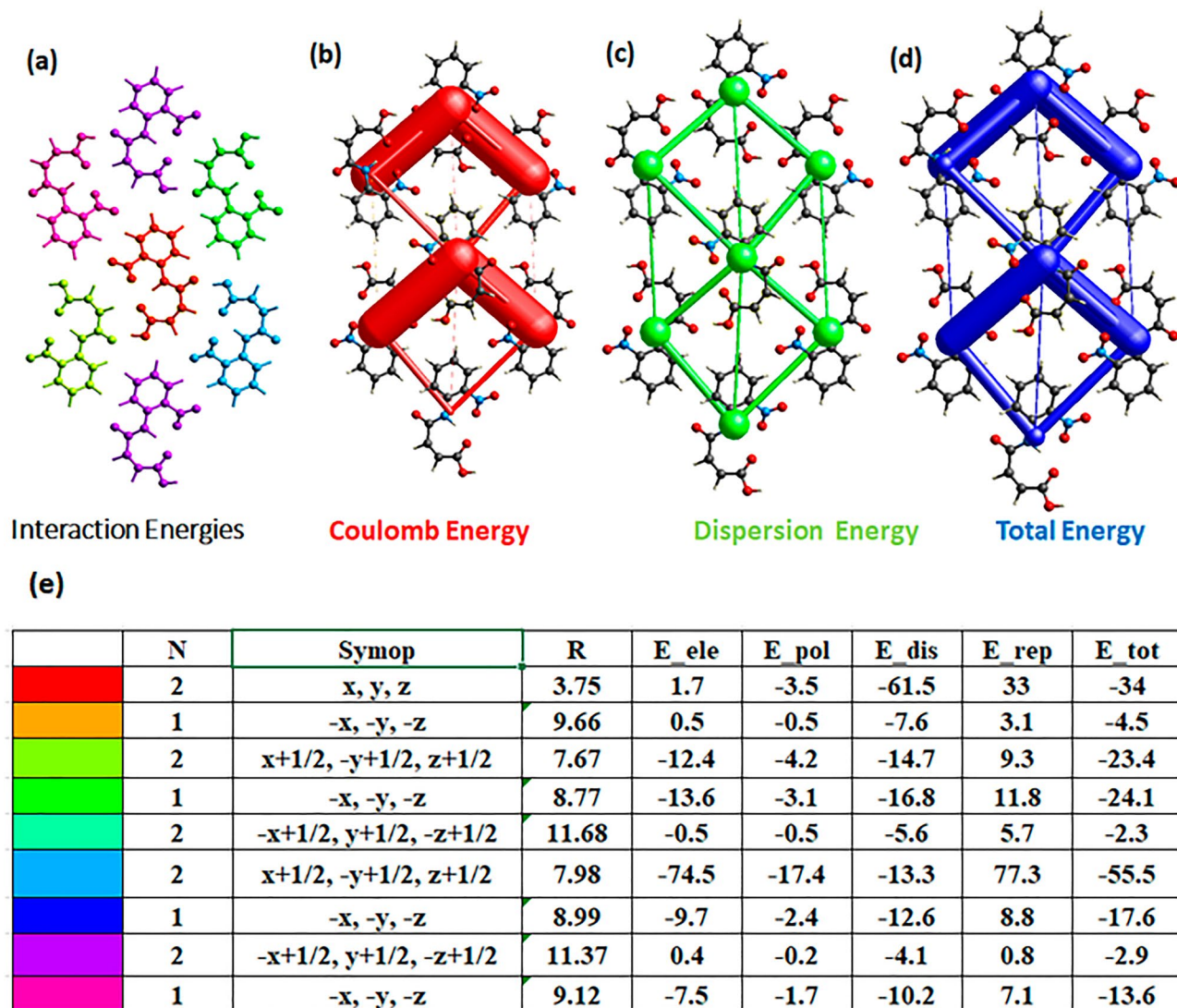
Fig. 10 **a** Interaction energies between the molecular pairs that lie within 3.8Å^3 of the reference molecule. Energy frameworks for **b** coulomb energy, **c** dispersion energy, **d** total energy. **e** Graphical view of the values of the various kind of interaction energies

	N	Symop	R	E_ele	E_pol	E_dis	E_rep	E_tot
	2	x, y, z	3.75	1.7	−3.5	−61.5	33	−34
	1	−x, −y, −z	9.66	0.5	−0.5	−7.6	3.1	−4.5
	2	x+1/2, −y+1/2, z+1/2	7.67	−12.4	−4.2	−14.7	9.3	−23.4
	1	−x, −y, −z	8.77	−13.6	−3.1	−16.8	11.8	−24.1
	2	−x+1/2, y+1/2, −z+1/2	11.68	−0.5	−0.5	−5.6	5.7	−2.3
	2	x+1/2, −y+1/2, z+1/2	7.98	−74.5	−17.4	−13.3	77.3	−55.5
	1	−x, −y, −z	8.99	−9.7	−2.4	−12.6	8.8	−17.6
	2	−x+1/2, y+1/2, −z+1/2	11.37	0.4	−0.2	−4.1	0.8	−2.9
	1	−x, −y, −z	9.12	−7.5	−1.7	−10.2	7.1	−13.6

geometry. Energy values for the multiple molecular orbitals from the HOMO to the fourth HOMO (HOMO – HOMO-3) and from the LUMO to the fourth LUMO (LUMO – LUMO + 3) were evaluated (Tables 4 and 5).

The analysis of the energy gaps between molecular orbitals (Table 5) revealed higher energy gaps for experimentally obtained crystal structure of the title compound comparing to the DFT-optimized geometry. This finding suggests that the experimental geometry of the compound has restricted mobility of the electrons and is less reactive. Overall low values of the dipole moment (Table 5) represent the nearly symmetrical charge distribution, when at the same time experimentally obtained structure possesses a slightly asymmetrical distribution of charges.

Last, the conceptual density functional theory (CDFT) was used to calculate the chemical reactivity descriptors that were originally introduced by Robert Parr [53–55], to provide a quantitative analysis of the investigated compound, and to provide an intrinsic understanding of the chemical and biological activities. Previously derived computational data for the HOMO and LUMO energy levels were utilized to find the global chemical reactivity descriptors, such as ionization potential (*IP*), electron affinity (EA), electronegativity (χ), chemical potential (μ), global hardness (η), global softness (σ), electrophilicity index (ω) and nucleophilicity index (*N*) (Table 6). The title compound possesses high ionization potential, electronegativity, and global hardness and nucleophilicity index

Fig. 11 Molecular orbitals diagrams for the experimental X-Ray obtained geometry (A) and DFT-optimized geometry of the title compound (values in eV)
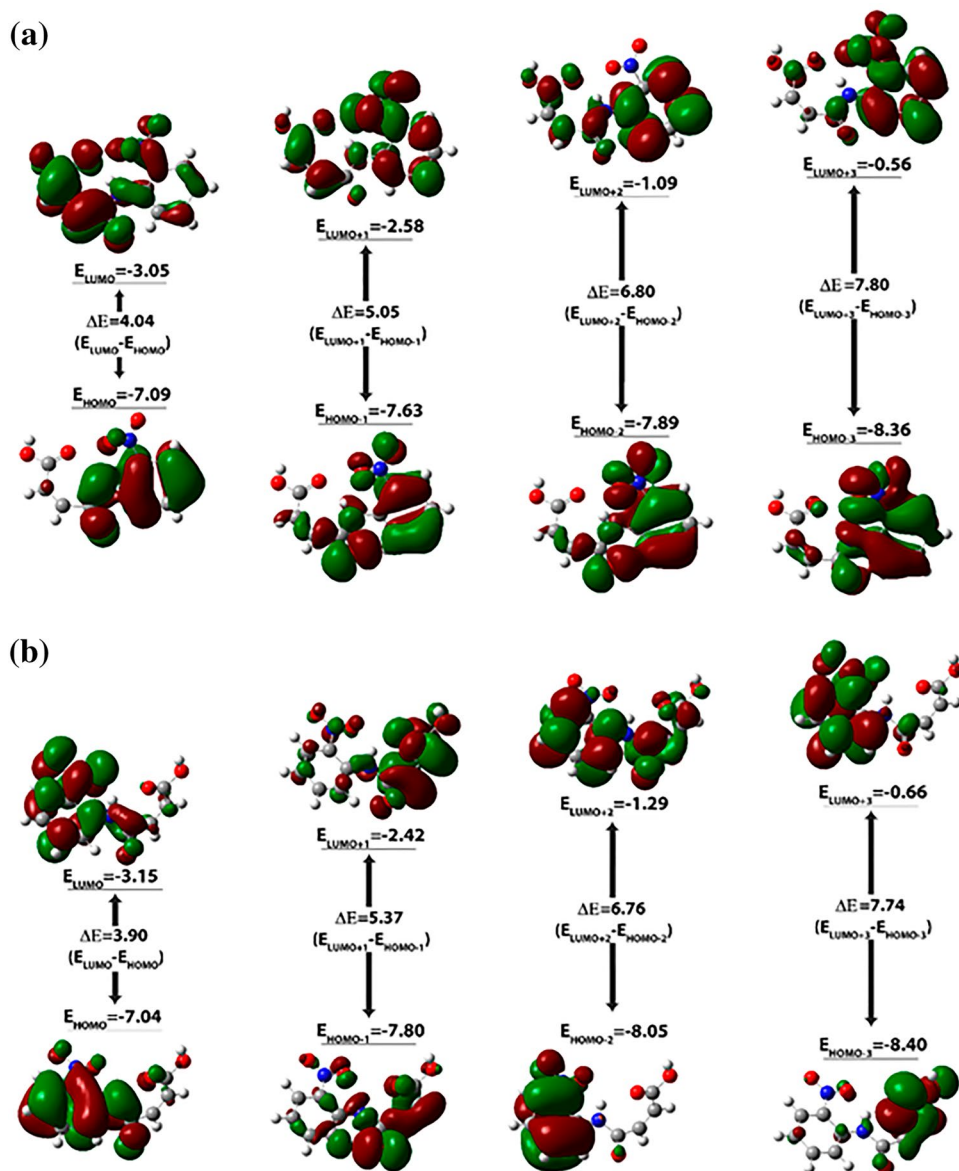
(a)

(b)

Table 4 Calculated energy values (in eV) for HOMO-3, HOMO-2, HOMO-1, HOMO, LUMO, LUMO + 1, LUMO + 2 and LUMO + 3 molecular orbitals for the title compound

X-Ray		Optimized	
LUMO + 3	−0.46	LUMO + 3	− 0.59
LUMO + 2	− 0.56	LUMO + 2	− 0.66
LUMO + 1	− 0.61	LUMO + 1	− 0.82
LUMO	− 0.94	LUMO	− 1.10
HOMO	− 5.92	HOMO	− 6.00
HOMO-1	− 6.15	HOMO-1	− 6.22
HOMO-2	− 6.69	HOMO-2	− 6.74
HOMO-3	− 6.96	HOMO-3	− 7.05

Table 5 Energy gaps (in eV), electronic energy (in eV) and dipole moment (in Debye) between calculated molecular orbitals for title compound

	X-RAY	Optimized
LUMO–HOMO	4.98	4.91
(LUMO + 1)-(HOMO-1)	5.54	5.41
(LUMO + 2)-(HOMO-2)	6.13	6.08
(LUMO + 3)-(HOMO-3)	6.50	6.46
E_{total}	− 23,714.18	− 23,719.39
Dipole moment	3.299515	1.111708

values, thus representing strong nucleophilic structure, that at the same time does not favor the change in the electron distribution. Supporting that, low escaping tendency

Table 6 Ionization potential (*IP*), electron affinity (*EA*), electronegativity (χ), chemical potential (μ), global hardness (η), global softness (σ), electrophilicity index (ω) and nucleophilicity index (*N*) for the title compound

	X-Ray	Optimized
IP	8.5081	8.3831
EA	0.8201	0.8110
χ	4.6641	4.5970
μ	− 4.6641	− 4.5970
η	7.6880	7.5721
σ	0.1301	0.1321
ω	1.4148	1.3954
N	2.4711	2.5079

of electrons is represented by low chemical potential value. In comparison with theoretically optimized geometry of the title compound, the experimentally obtained structure has slightly stronger pronounced properties of nucleophilic structure.

Conclusion

The crystalline anilide, i.e., (Z)-4-((2-nitrophenyl)amino)-4-oxobut-2-enoic acid (**NAOB**) was synthesized by using the reported method and experimental and theoretical investigation were performed. The structure of **NAOB** was unambiguously confirmed by the SC-XRD technique which showed that the molecular configuration was stabilized by intramolecular N–H ⋯ O bonding. The crystal packing was stabilized by O–H ⋯ O, C–H ⋯ O and offset $\pi \cdots \pi$ stacking interactions. Hirshfeld surface analysis inferred that O ⋯ H contact was the most significant contributor of the crystal packing. The crystal packing environment was further explored by the interaction energy between the molecular pairs which showed that the dispersion energy played dominant role for the stabilization of solid-state assembly. The DFT calculations performed to analyze the chemical and physical properties of the **NAOB** demonstrated the comparable energy states of the experimentally obtained crystal structure and the computationally optimized structure, but increased energy gaps between LUMO and HOMO molecular orbitals for the experimentally obtained crystal structure, revealing the lower mobility of the electrons and insignificant asymmetrical distribution of charges. The chemical reactivity descriptors obtained upon quantification analysis of the energy gaps between molecular orbitals demonstrated that **NAOB** possesses strong nucleophilic properties that are even stronger pronounced than those for the theoretically optimized structure.

Declarations

References

1. M.A. El-Hashash, S.A. Rizk, S.R. Atta-Allah, Molecules **20**, 22069 (2015). https://doi.org/10.3390/molecules201219827
2. M. Bianchi, A. Butti, Y. Christidis, J. Perronnet, F. Barzaghi, R. Cesana, A. Nencioni, Eur. J. Med. Chem. **23**, 45 (1988). https://doi.org/10.1016/0223-5234(88)90166-3
3. M.D. Vitorović-Todorović, A. Erić-Nikolić, B. Kolundžija, E. Hamel, S. Ristić, I.O. Juranić, B.J. Drakulić, Eur. J. Med. Chem. **62**, 40 (2013). https://doi.org/10.1016/j.ejmech.2013.01.006
4. M. Bazargan, F. Ghaemi, A. Amiri, M. Mirzaei, Coord. Chem. Rev. **445**, 214107 (2021). https://doi.org/10.1016/j.ccr.2021.214107
5. M. Bazargan, M. Mirzaei, A. Franconetti, A. Frontera, Dalton Trans. **48**, 5476 (2019). https://doi.org/10.1039/C9DT00542K
6. R. Khajavian, M. Mirzaei, H. Alizadeh, Dalton Trans. **49**, 13936 (2020). https://doi.org/10.1039/D0DT02798G
7. P. Theivendren, A. Subramanian, I. Murugan, S.D. Joshi, U.A. More, Chem. Biol. Drug Des. **89**, 714 (2017). https://doi.org/10.1111/cbdd.12894
8. T. Panneerselvam, S. Arumugam, M.A. Ali, K. Selvaraj, M. Indhumathy, A. Sivakumar, S.D. Joshi, ChemistrySelect **2**, 2341 (2017). https://doi.org/10.1002/slct.201601763
9. W. Kemnitzer. S. Cai. J. Drewe, N. Sirisoma, Google Patents2008.
10. M.J. Kukla, H.J. Breslin, C.J. Diamond, P.P. Grous, C.Y. Ho, M. Miranda, J.D. Rodgers, R.G. Sherrill, E. De Clercq, R. Pauwels, K. Andries, L.J. Moens, M.A.C. Janssen, P.A.J. Janssen, J. Med. Chem. **34**, 3187 (1991). https://doi.org/10.1021/jm00115a007
11. A. Hassanpoor, M. Mirzaei, H. Eshtiagh-Hosseini, A. Majcher, CrystEngComm **20**, 3711 (2018). https://doi.org/10.1039/C8CE00573G
12. H. Eshtiagh-Hosseini, M. Mirzaei, M. Biabani, V. Lippolis, M. Chahkandi, C. Bazzicalupi, CrystEngComm **15**, 6752 (2013). https://doi.org/10.1039/C3CE40743H
13. A. Ali, M. Khalid, M.F.U. Rehman, S. Haq, A. Ali, M.N. Tahir, A.A.C. Braga, ACS Omega **5**, 15115 (2020). https://doi.org/10.1021/acsomega.0c00975
14. A. Ali, Z.U. Din, M. Ibrahim, M. Ashfaq, S. Muhammad, D. Gull, M.N. Tahir, E. Rodrigues-Filho, A.G. Al-Sehemi, M. Suleman, RSC Adv. **13**, 4476 (2023). https://doi.org/10.1039/D2RA07681K
15. A. Ali, M. Ashfaq, Z.U. Din, M. Ibrahim, M. Khalid, M.A. Assiri, A. Riaz, M.N. Tahir, E. Rodrigues-Filho, M. Imran, A. Kuznetsov, ACS Omega **7**, 39294 (2022). https://doi.org/10.1021/acsomega.2c05441
16. O. Simsek, M. Ashfaq, M.N. Tahir, S. Ozturk, E. Agar, J. Struct. Chem. **64**, 942 (2023). https://doi.org/10.1134/S002247662305012 8
17. S.L. Rubab, A.R. Raza, B. Nisar, M. Ashfaq, Y. Altaf, R. Hussain, H.M. Ali, Molecules **28**, 4375 (2023). https://doi.org/10.3390/molecules28114375
18. R.K. Askerov, M. Ashfaq, E.V. Chipinsky, V.K. Osmanov, M.N. Tahir, E.V. Baranov, G.K. Fukin, V.N. Khrustalev, R.H. Nazarov, G.N. Borisova, Z.V. Matsulevich, A.M. Maharramov, A.V. Borisov, Results Chem. **4**, 100600 (2022). https://doi.org/10.1016/j.rechem.2022.100600
19. A. Hassanpoor, M. Mirzaei, M. Niknam Shahrak, A.M. Majcher, Dalton Trans. **47**, 13849 (2018). https://doi.org/10.1039/C8DT02986E

20. P. Praveen Kumar, Y. Dathu Reddy, C.V.R. Reddy, B.R. Devi, P.K. Dubey, Org. Chem. Int. **2014**, 1 (2014). https://doi.org/10.1155/2014/576715

21. G.M. Sheldrick, Acta Crystallogr. Sect. A: Found. Adv. **71**, 3 (2015). https://doi.org/10.1107/S2053273314026370

22. G.M. Sheldrick, Acta Crystallogr. C Struct. Chem. **71**, 3 (2015). https://doi.org/10.1107/S2053229614024218

23. L.J. Farrugia, J. Appl. Crystallogr. **45**, 849 (2012). https://doi.org/10.1107/S0021889812029111

24. A.L. Spek, Acta Crystallogr. D Biol. Crystallogr. **65**, 148 (2009). https://doi.org/10.1107/S090744490804362X

25. C.F. Macrae, I. Sovago, S.J. Cottrell, P.T. Galek, P. McCabe, E. Pidcock, M. Platings, G.P. Shields, J.S. Stevens, M. Towler, J. Appl. Crystallogr. **53**, 226 (2020). https://doi.org/10.1107/S1600576719014092

26. M. Frisch, G. Trucks, H. Schlegel, G. Scuseria, M. Robb, J. Cheeseman, G. Scalmani, V. Barone, G. Petersson, H. Nakatsuji, Revision A **3**, 310 (2016)

27. R. Dennington. T. A. Keith, J. M. Millam, Semichem Inc.: Shawnee Mission, KS, USA (2016).

28. A. Ali, M. Khalid, Z.U. Din, H.M. Asif, M. Imran, M.N. Tahir, M. Ashfaq, E. Rodrigues-Filho, J. Mol. Struct. **1241**, 130685 (2021). https://doi.org/10.1016/j.molstruc.2021.130685

29. T. Lu, F. Chen, J. Comput. Chem. **33**, 580 (2012). https://doi.org/10.1002/jcc.22885

30. J. Bernstein, R.E. Davis, L. Shimoni, N.L. Chang, Angew. Chem. Int. Ed. Engl. **34**, 1555 (1995). https://doi.org/10.1002/anie.199515551

31. M. Mirzaei, H. Eshtiagh-Hosseini, Z. Karrabi, K. Molčanov, E. Eydizadeh, J.T. Mague, A. Bauzá, A. Frontera, CrystEngComm **16**, 5352 (2014). https://doi.org/10.1039/C4CE00325J

32. H. Eshtiagh-Hosseini, M. Mirzaei, S. Zarghami, A. Bauzá, A. Frontera, J.T. Mague, M. Habibi, M. Shamsipur, CrystEngComm **16**, 1359 (2014). https://doi.org/10.1039/C3CE41730A

33. C.R. Groom, I.J. Bruno, M.P. Lightfoot, S.C. Ward, Acta Crystallogr Sect. B: Struct. Sci. Cryst. Eng. Mater. **72**, 171 (2016). https://doi.org/10.1107/S2052520616003954

34. J.L. Wardell, J.M. Skakle, J.N. Low, C. Glidewell, Acta Crystallogr Sect. E: Struct. Rep. Online **61**, o3849 (2005). https://doi.org/10.1107/S160053680503374X

35. B.T. Gowda, M. Tokarčík, K. Shakuntala, J. Kožíšek, H. Fuess, Acta Crystallogr Sect. E: Struct. Rep. Online **66**, o1671 (2010). https://doi.org/10.1107/S1600536810022245

36. P.R. Spackman, M.J. Turner, J.J. McKinnon, S.K. Wolff, D.J. Grimwood, D. Jayatilaka, M.A. Spackman, J. Appl. Crystallogr. **54**, 1006 (2021). https://doi.org/10.1107/S1600576721002910

37. M.A. Spackman, D. Jayatilaka, CrystEngComm **11**, 19 (2009). https://doi.org/10.1039/B818330A

38. S.A. Al-Jibori, G.H.H. Al-Jibori, M. Ashfaq, T. Khalil, M. Laguna, C. Wagner, M.N. Tahir, A.S.M. Al-Janabi, J. Mol. Struct. (2023). https://doi.org/10.1016/j.molstruc.2023.135803

39. A.S. Faihan, R.H. AlShammari, M. Ashfaq, S. Muhammad, S.A. Al-Jibori, M.N. Tahir, M.R. Hatshan, A.S. Al-Janabi, S.M. Al-Moayid, J. Mol. Struct. **1286**, 135633 (2023). https://doi.org/10.1016/j.molstruc.2023.135633

40. J.J. McKinnon, D. Jayatilaka, M.A. Spackman, ChemComm. (2007). https://doi.org/10.1039/B704980C

41. M. Haroon, M.W. Baig, T. Akhtar, M.N. Tahir, M. Ashfaq, J. Mol. Struct. **1287**, 135692 (2023). https://doi.org/10.1016/j.molstruc.2023.135692

42. M. Kurbanova, M. Ashfaq, M.N. Tahir, A. Maharramov, N. Dege, N. Ramazanzade, E.B. Cinar, J. Struct. Chem. **64**, 437 (2023). https://doi.org/10.1134/S0022476623030095

43. M. Mirzaei, H. Eshtiagh-Hosseini, A. Bauzá, S. Zarghami, P. Ballester, J.T. Mague, A. Frontera, CrystEngComm **16**, 6149 (2014). https://doi.org/10.1039/C4CE00003J

44. Z. Hosseini-Hashemi, M. Mirzaei, A. Jafari, P. Hosseinpour, M. Yousefi, A. Frontera, M.L. Dashtbayaz, M. Shamsipur, M. Ardalani, RSC Adv. **9**, 25382 (2019). https://doi.org/10.1039/C9RA05143K

45. M. Mirzaei, H. Eshtiagh-Hosseini, M. Shamsipur, M. Saeedi, M. Ardalani, A. Bauzá, J.T. Mague, A. Frontera, M. Habibi, RSC Adv. **5**, 72923 (2015). https://doi.org/10.1039/C5RA09526C

46. M.J. Turner, J.J. McKinnon, D. Jayatilaka, M.A. Spackman, CrystEngComm **13**, 1804 (2011). https://doi.org/10.1039/C0CE00683A

47. M.N. Tahir, A. Ali, M. Khalid, M. Ashfaq, M. Naveed, S. Murtaza, I. Shafiq, M.A. Asghar, R. Orfali, S. Perveen, Molecules **28**, 2967 (2023). https://doi.org/10.3390/molecules28072967

48. W.A. Shehnaz, A. Siddiqui, M. Ashraf, M.N. Ashfaq, S.N. Tahir, Appl. Organomet. Chem. **37**, e7077 (2023). https://doi.org/10.1002/aoc.7077

49. C.F. Mackenzie, P.R. Spackman, D. Jayatilaka, M.A. Spackman, IUCrJ **4**, 575 (2017). https://doi.org/10.1107/S2052252517000848X

50. M.J. Turner, S. Grabowsky, D. Jayatilaka, M.A. Spackman, J. Phys. Chem. Lett. **5**, 4249 (2014). https://doi.org/10.1021/jz502271c

51. M. Kurbanova, M. Ashfaq, M.N. Tahir, A. Maharramov, N. Dege, A. Koroglu, J. Struct. Chem. **64**, 302 (2023). https://doi.org/10.1134/S0022476623020142

52. A. Ali, M. Khalid, S. Abid, M.N. Tahir, J. Iqbal, M. Ashfaq, F. Kanwal, C. Lu, M. F. u. Rehman, Crystals **10**, 778 (2020). https://doi.org/10.3390/cryst10090778

53. R.G. Parr, in *Horizons of Quantum Chemistry*. ed. by K. Fukui, B. Pullman (Springer, Netherlands, Dordrecht, 1980)

54. R.G. Parr, R.A. Donnelly, M. Levy, W.E. Palke, J. Chem. Phys. **68**, 3801 (2008). https://doi.org/10.1063/1.436185

55. R.G. Parr, R.G. Pearson, J. Am. Chem. Soc. **105**, 7512 (1983). https://doi.org/10.1021/ja00364a005

Authors and Affiliations

Muhammad Ashfaq[1] [ORCID] · **Muhammad Nawaz Tahir[1]** · **Georgii Bogdanov[2]** · **Akbar Ali[3]** · **Muhammad Ahmed[1]** · **Gulzar Ahmed[4]** · **Anees Abbas[5]**

✉ Muhammad Ashfaq
  ashfaq.muhammad@uos.edu.pk;
  muhammadashfaq1400@gmail.com

✉ Gulzar Ahmed
  gulzarahmed_physics@yahoo.com

[1] Department of Physics, University of Sargodha, Sargodha 40100, Pakistan

[2] Department of Chemical and Biomolecular Engineering, University of California Irvine, Irvine, CA 92697, USA

[3] Department of Chemistry, Government College University Faisalabad, Faisalabad 38000, Pakistan

[4] South China University of Technology, Material Science and Engineering, Guangzgou, China

[5] Department of Chemistry, University of Mianwali, Mianwali 42200, Pakistan